3D morphological analysis of copper foams as current collectors for Li-ion batteries by means of X-ray tomography

A. Etiemble, J. Adrien, E Maire, H. Idrissi, D. Reyter, L. Roué

3D morphological analysis of copper foams as current collectors for Li-ion batteries by means of X-ray tomography

A. Etiemble[a,b], J. Adrien[a], E. Maire[a,*], H. Idrissi[a], D. Reyter[b] L. Roué[b,**]

[a] *Institut national des sciences appliquées de Lyon, Laboratoire MATEIS, F-69621 Villeurbanne, France.*

[b] *Institut national de la recherche scientifique – Centre Énergie, Matériaux, Télécommunications, Varennes, Québec, J3X 1S2, Canada*.

Corresponding authors at:

* INSA–Lyon MATEIS CNRS UMR5510, F–69621 Villeurbanne, France Tel.: +33 4 72 43 88 61.

** INRS–Énergie, Matériaux et Télécommunications, 1650, bd. Lionel Boulet, Varennes, Québec, J3X1S2 Canada. Tel.: +1 514 228 6985.

E–mail addresses: eric.maire@insa–lyon.fr (E. Maire), roue@emt.inrs.ca (L. Roué)

Abstract

As-received and chemically treated copper foams were characterized by means of laboratory X-ray tomography with a resolution of 0.5 µm. 3D image processing and analysis allowed the morphological parameters (size, sphericity, tortuosity…) of the pores and copper skeleton to be determined. The chemical dissolution of the Cu foam in an acid hydrogen peroxide solution results in an increase of the open pore size (from 54 to 93 µm) and a decrease of the foam thickness (from 140 to 115 µm). With an open porosity of 81.8% and a specific surface area as high as 280,000 (49,000) m^2 m^{-3} of Cu (foam), the chemically-treated Cu foam appears very attractive for use as a 3D current collector for metal (*e.g.* Si) based anodes for Li-ion batteries.

Keywords: *3D morphology, X-ray tomography, Cu foam, Li-ion batteries*

1. Introduction

Metallic foams are used in numerous industrial applications such as light-weight structures, biomedical implants, filters, electrodes, catalysts or heat exchangers. In particular, electrodes for Ni-MH and Ni-Cd batteries are among the largest industrial applications of metallic foams nowadays **[1]**. Several authors have recently demonstrated interest in the use of copper foams as substrates for Si and Sn based anodes for Li-ion batteries **[2-5]**. Thanks to its interconnected 3D architecture, a Cu foam acts as an efficient current collector and a rigid matrix for the active Si or Sn material, which suffers from important volume changes with cycling. As a result, these 3D anodes display a better cycle life in comparison with common 2D anodes prepared on flat Cu foil. The gravimetric and volumetric capacities of these electrodes are, however, affected by the non-reactive 3D substrate. The amount of porosity, the connectivity of the porous network, the pore size and shape, the foam thickness, the surface roughness and specific surface area are all key parameters for the optimization of foams to be employed as a Li-ion anode substrate (current collector).

Metallic foams with high open porosity (>80%) can be produced using different processes (*e.g.* impregnation of a porous body with a liquid metal, deposition of metals on polymeric foams, electrodeposition of metal with concomitant hydrogen gas evolution) **[1].** However, the production of thin (< 0.5 mm) and highly porous metal foams as required for Li-ion battery application is challenging. The common method to decrease the thickness of foam-based electrodes is to calendar the electrode after loading the foam with the active material but this results in an electrode with a low active

material/current collector mass ratio, which hinders practical application in Li-ion batteries **[5].**

Highly porous copper foams made by Metafoam technologies Inc. have recently shown great performance in heat pipes for electronic cooling **[6]**. Their manufacturing is based on an innovative powder metallurgy process **[7]**. It allows producing open-cell foams with unique microstructure exhibiting a much larger specific surface area (up to 100,000 m^2 m^{-3}) than that of usual metallic foams. This is a valuable advantage for battery applications. However, their density and thickness must be reduced for an optimal use as a Li-ion anode substrate. For that purpose, their partial chemical dissolution, as described in the present study, appears as a simple and efficient approach.

X-ray tomography is a powerful non-destructive technique which can provide 3D images of complex microstructures **[8,9]**, especially in the case of highly porous materials **[10-16]**. Recently, several studies have demonstrated its interest for ex-situ and in-situ imaging of battery materials **[17-27].** The development of 3D imaging software has greatly favored automatic processing and they now allow quantitative measurements by finite element calculations or other numerical models **[28-30]**. The maximum spatial resolution of the technique can reach about 30 nm with synchrotron tomography, but remains currently limited to 1.0 µm with laboratory tomography systems **[31]**.

In this study, a tridimensional morphological analysis of open-cell copper foams is performed by means of laboratory X-ray tomography with a resolution of 0.5 µm which is, to the best of our knowledge, amongst the highest resolutions obtained with this type of equipment. The morphological parameters (pore size, tortuosity, specific surface area…) of the foam structure are determined. The effect of a chemical dissolution

treatment on the foam morphological characteristics is highlighted. The interest of these Cu foams for use as 3D current collectors for Li-ion batteries is discussed on the basis of their morphological characteristics.

2. Experimental

2.1. Materials

The copper metal foams provided by Metafoam Technologies Inc. consist of 16 x 160 mm strips with a thickness of about 150-200 µm. The relative density of the as-received foam (estimated from mass and size measurements) was about 20%. 1 cm^2 discs of this foam were stamped for this study. Acid hydrogen peroxide, commonly used as a copper etching solution **[32],** was used for the chemical dissolution treatment. Disk foam samples were immersed for 180 s in a freshly prepared 15 mL stirred aqueous solution of 1M HCl + 0.4M H_2O_2 at 50°C. The copper foam was then washed of the corrosion products by immersing it in distilled water with ultrasound for 30 s at room temperature. Finally, the sample was annealed for 3 h at 300°C in an Ar/H_2 (5%) atmosphere. Mass measurement of the foam sample before and after the dissolution treatment indicated a mass decrease of ~30%. Besides, no residual salts were detected by energy dispersive X-ray (EDX) analysis on the dissolved Cu foam. Note that a higher mass decrease (*i.e.* thinner and more porous foam) can be obtained by increasing the immersion time but the resulting foam is too fragile. Besides, comparative tests with and without stirring of the acid hydrogen peroxide solution indicated that the stirring is required to have uniform dissolution of the foam.

2.2. X-ray tomography analysis

X-ray tomography consists in acquiring a series of X-ray radiographs of a sample that rotates around an axis perpendicular to the incident beam. The spatial density distribution is then reconstructed by using a standard filtered back-projection algorithm **[30]**. Detailed analysis of the foam morphology before and after chemical dissolution was performed using a laboratory tomograph designed by the company RX Solution LTD. A very high resolution (compared to currently available cone beam laboratory systems) is achieved by using a new Hammamatsu X-ray Source. It achieves a spot size of 0.7 µm when using a W filamnet and it can even be reduced to 0.25 µm with a LaB_6 cathode.

The X-ray source was operated with a LaB_6 cathode at a voltage of 100kV. The detector was a Hamamatsu CMOS Flat Panel with a pixel size of 50µm. The samples were scanned at a voxel size of 0.5µm. Each scan consisted in 900 projections with an exposure time of 5s and an averaging of 3 radiographs for each.

3. Results

3.1. Scanning electron microscopy (SEM) analysis

Fig. 1 shows SEM micrographs of the surface and cross-section for as-received (A-C) and dissolved foams (D-F). The untreated foam has a spherical cluster structure with particle diameter of 10-50 µm. No ligaments can be observed, unlike other types of metal foams. This morphology provides a large-scale open porosity and a high surface area **[6]**. After dissolution, the cluster structure is retained but the particles appear less spherical and much rougher (see **Fig. 1C** *versus* **1F**). The porosity seems larger and the foam

thickness decreases from about 150 to 120 µm thick on the basis of the cross-sectional images shown in **Fig. 1B** and **1E**).

3.2. Threshold processing of the X-ray tomogram images

A key step of the process to reconstruct the 3D structure is the segmentation which separates all the voxels of the image into two families (black and white) **[15,30]**. A grey-scale X-ray density image of a slice of the untreated foam is shown in **Fig. 2A**. The intensity frequency histogram of the grey levels (**Fig. 2B**) shows two distinct peaks associated with the two phases (gaseous and solid). The output of this processing step should resemble as closely as possible the actual microstructure of the sample. The attenuation coefficient of the Beer-Lambert law, which is used in X-ray radiography physics, is proportional to the fourth power of the atomic number (Z^4) and the density (ρ) of the investigated material **[9]**. The contrast observed in the X-ray radiograph is explained by this attenuation law. Also, due to the rather high atomic number of the copper, the grey level (intensity) can be quite easily divided into two families, thanks to the strong difference in the attenuation coefficient between the solid and the gaseous phase. The intensity (140) at the minimum between the two peaks of the histograms (**Fig. 2B**) is selected as threshold between the solid and gas phases. After processing (**Fig. 2C**), the white and black families have to be understood as belonging to the copper matrix and the gaseous phase contained in the porosity, respectively. The comparison between the grey-scale (**Fig. 2A**) and binary (**Fig. 2C**) images visually confirms that the two phases can be precisely identified.

3.3. 3D Representation

Fig. 3 shows the 3D view of the as-received (**A-B**) and dissolved (**C-D**) copper foam. Videos of both 3D architectures are presented in the Supplementary Material section. As previously observed on the SEM images, the initial foam is composed of many spherical clusters, welded together through thinner bonds, forming a well-connected and tortuous structure. After the dissolution, larger porosities are noticeable and the bonds between the particle clusters are less abundant and thinner than for the initial structure. In addition, many cavities are observed on the particle surface that could be associated with the opening of the intra-particle porosity during the chemical treatment.

In order to confirm these qualitative visualizations, 3D quantitative analyses have been performed. The porosity can be quantitatively represented by a surface mapping of the copper fraction through the perpendicular direction. This is calculated by counting the fraction of white voxels along the thickness (z-axis) of the sample. This can be achieved for each column of voxels and plotted in a 2D image with dimensions (x,z) equal to these of the sample. This 2D image of the fraction along the thickness is named the 'surface mapping'. More simply, the porosity can also be calculated in slices perpendicular to the three main axis (x,y and z) and then plotted as density value profiles along these axes. The open- and closed- pores can be identified and the morphological parameters (size, sphericity, tortuosity…) of each object (open pore, closed pore and copper matrix) can be determined. These different aspects are described in the following sections and the different morphological parameters determined for the as-received and dissolved foams are summarized in **Tables 1 and 2**.

3.4. Porosity distribution

A surface mapping of the porosity has first been calculated. The studied volumes have been reduced to dimensions equal to (500 µm x 750 µm x average thickness). This helped to minimize the amount of gaseous phase outside of the copper foam so it leads to a better counting of the porosity, excluding the outside air. The mapping can be made by counting the number of black (white) voxels along the direction perpendicular to the surface of the sheet and dividing the sum by the average thickness expressed in voxels (280 and 230 for the as-received and dissolved foams, respectively).

Fig. 4 presents a color mapping of this through-thickness porosity in the (xy) and (yz) plans for the as-received (**A**) and dissolved (**B**) foams. In both cases, the porosity distribution in the (xy) plan is quite inhomogeneous (~10-100%). For the dissolved foam (**Fig. 4B**), high porosity zones are clearly more numerous than for the as-received foam (**Fig. 4A**). Indeed, ~29% of the dissolved foam surface corresponds to pores traversing the foam thickness compared to ~9% for the untreated foam. Regarding the (yz) plan, it appears that the thickness of the dissolved foam is lower and less regular than for the as-received foam. However, no significant gradient in the mean porosity is observed from the surface to the center of the dissolved foam, suggesting that its dissolution is uniform. The average porosity equals 72.1% for the initial foam compared to 82.1% for the dissolved sample, confirming the efficiency of the dissolution procedure to increase the foam porosity. This is also supported by comparing typical porosity profiles of the as-received and dissolved foams as shown in **Fig. 5** in the x (**A**), y (**B**) and z (**C**) directions. For both samples, the surface porosity fluctuates slightly along the x and y directions

with a relative standard deviation $RSD_x = RSD_y = 6\%$. The porosity in the z-direction (*i.e.* in the thickness direction) (**Fig. 5C**) appears quite stable in the center of the specimen. It increases quickly at the surface between the foam and the air. The porosity profiles along the 3 directions confirm the increase of the foam porosity with the dissolution treatment. In addition, the z-direction profile width (**Fig. 5C**) is lower for the dissolved foam (115 µm *vs.* 140 µm for the as-received foam), confirming the decrease of the foam thickness during the dissolution treatment.

3.5. Open- and closed- porosities

The connectivity of each selected phase (solid or gaseous) can be determined by a counting procedure detecting the 3D independent objects as described in **[11]**. Each object, defined as a cluster of connected voxels, can then be labeled by a different grey level on resulting tomographic slices. **Fig. 6** shows a typical slice in the plane of the sheets for the as-received foam obtained according to this procedure. The closed-porosity forming small objects (white zones) in the copper matrix (black zone) can be distinguished from the open-porosity (grey zone). For the as-received foam, the open-porosity and closed-porosity represent respectively 71.1 and 1.0% of the total analyzed volume (500 µm x 750 µm x thickness) compared to 81.8 and 0.3% for the dissolved foam (**Table 1**).

3.6. Pore morphological parameters

The morphological parameters of the closed or open pores (sphericity, size and tortuosity) can be determined by various methods. The pore sphericity, SP, can be calculated from the volume, V, and surface area, S, according to the formula **[11]**:

$$SP = 6V\sqrt{\frac{\pi}{S^3}} \quad (1)$$

This parameter is equal to 1 for a sphere and less for any other shape. The sphericity of the open- and closed-pores is given in **Table 1** for the as-received and dissolved foams. In both cases, the SP value of the open-pores is very low (SP = 0.07-0.14) confirming their irregular shape whereas the closed-pores are relatively spherical in shape (SP = 0.66-0.78).

The pore size distribution can be measured using sequential opening operations. This process consists in a combination, with successive structural elements of size (n), of image erosion followed by dilation. Erosion and dilation are very straightforward operations applied to a binary image during an image processing procedure. They consist in removing (respectively adding) a layer of white pixels at the interface of each white object in the image. The difference between the dilated and the initial image allows retrieving the fraction of elements of thickness 2n in the image **[16]**. The pore size calculation can be obtained from the use of cubic, spherical or octahedral elements, but the process with octahedral elements gives a larger equivalent diameter, which is generally more realistic **[16]**. **Fig. 7** shows the cumulative size distributions of the open and closed pores for the as-received and dissolved foams. As expected, the sizes of the open-pores are larger for the dissolved foam with a median value of 93 µm *versus* 54 µm

for the as-received foam. In contrast, the size distribution of the closed-pores is similar for both foams with a median value of ~6 µm (**Table 1**).

The tortuosity of the porosity is defined as the ratio of the distance to go from one point of the microstructure to another while keeping inside of the gaseous phase divided by the straight distance between these two points. In other words, it corresponds to the deviation of the straight path imposed by the presence of the particles composing the foam. The tortuosity can be determined from labelled trajectories followed through the network, starting from an initial seed plane located in the middle of the 3D data set, as described elsewhere **[16]**. The neighbor number of each voxel during the grown processing can be fixed at 6 (shared sides) or 26 (shared sides, edges and summits), which respectively overestimates and underestimates the tortuosity. It can be considered that the most reasonable value can be obtained by using the average of 6 and 26 neighbors. The tortuosities for the initial and dissolved foam samples are isotropic in the three Cartesian directions. For both samples, the tortuosity of the porosity is close to 1 (**Table 1**).

3.7. Copper morphological parameters

The thickness, specific surface area, sphericity and tortuosity of the copper phase can be determined by the same method applied to the porosity in the previous sections. These morphological parameters are summarized in **Table 2**. As observed previously on the SEM images (**Fig. 1**) and 3D representation (**Fig. 3**), the copper matrix consists of a spherical cluster structure. The copper particles are well welded, inducing low sphericity of the copper phase. For both foams, the copper thickness exhibits a Gaussian distribution

(**Fig. 8**), centered on 14.5 µm. The tortuosity of the copper matrix is around 1.2 and isotropic in the three Cartesian directions for both foams.

Finally, the as-received foam provides a very large specific surface area (~74,000 m^2/m^3) in accordance with the manufacturer's claims. The specific surface area of the dissolved foam is lower (~49,000 m^2/m^3). However, related to the copper volume rather than the total foam volume, the specific surface area is slightly higher for the dissolved foam (~280,000 m^2/m^3_{Cu}) than initially (~260,000 m^2/m^3_{Cu}). This result indicates that the decrease of the specific surface area of the dissolved foam is related to the decrease of the amount of copper. In addition, due to the X-ray tomography resolution (0.5 µm), the specific surface area values are probably underestimated, especially for the dissolved foam, which presents a rougher surface (**Fig. 1F**) compared to the initial foam (**Fig. 1C**).

4. Discussion

The as-received copper foam exhibits promising morphological characteristics for use as a substrate (current collector) for metal-based anodes for Li-ion batteries. Indeed, the well-connected 3D structure, acting as a rigid matrix, should help to maintain the mechanical integrity of the composite electrode despite the large volume changes of the active material with cycling. This 3D architecture also offers the possibility to elaborate thick electrodes (*i.e.* having high areal mass loadings to reach high surface capacities) which tend to delaminate during the coating process when deposited on traditional flat current collectors **[33]**. Moreover, its high specific surface area (~74,000 m^2/m^3) may allow good electrical contact between the active material and the current collector. It is well known that the tortuosity of porous electrodes affects their mass transport properties

since the effective conductivities and diffusivities of the electrolyte in a porous electrode are inversely proportional to its tortuosity **[19,34]**. In the present case, the tortuosity of the pores (~1.0) and copper matrix (~1.2) is low, limiting the effects of this parameter on the electrode properties. In other words, the mass transport properties of the electrode will depend on the tortuosity of the porous network in the (active material + conductive additive + binder) composite incorporated into the foam rather than that of the foam itself. The relatively high open-porosity (71.1%) of the as-received foam limits its mass (volume) proportion to the total mass (volume) of the electrode, which has a positive impact on its gravimetric (volumetric) storage capacity. However, with a mean thickness of 140 µm and a density of 2.5 g cm^{-3}, the areal mass of the as-received foam (35 mg cm^{-2}) is still too high compared with that a flat current collector (18 mg cm^{-2} for a 20 µm thick Cu foil).

The dissolution of the copper foam in a chloride acidic hydrogen peroxide solution induces an important increase of the open-pore size (90 µm *versus* 54 µm for the as-received foam) resulting in a significant increase of the open-pore porosity (80.7% *versus* 71.1% for the as-received foam). A decrease of the foam thickness is also observed (115 µm *versus* 140 µm for the as-received foam). The dissolution procedure being done under vigorous stirring of the bath, the foam dissolution should be uniform. This is also favored by the relatively high porosity and low thickness of the initial foam, limiting diffusion constraints in the foam. Consequently, the decrease of the foam thickness is assumed to mainly result from the collapse of the Cu skeleton rather than from preferential dissolution of both sides of the foam. Note that the collapse of the Cu skeleton must also be accentuated by the ultrasonic treatment done during the washing procedure. As a

result, the dissolved foam has an areal mass as low as 18.4 mg cm^{-2}, which is comparable to that of a 20 µm thick Cu foil. Such a foam is thus very attractive to produce 3D battery electrodes with high gravimetric and volumetric capacities. On the other hand, no major modification of the other morphological parameters of the copper foam (copper skeleton thickness, sphericity, tortuosity) is observed with the dissolution treatment. This tends to confirm that the increase of the foam porosity mainly results from the collapse of the Cu skeleton through the dissolution of the thin bonds that joined the spherical Cu particles (**Fig. 1**). In addition, it appears that the copper surface is rougher after the dissolution treatment (**Fig. 1F**). This may be favorable for improving the adhesion of the electrode composite coating on the current collector resulting in an increase of the electrode cycle life, as observed with Si-based electrodes made with a roughened Cu current collector **[35]**. The electrical conductivity of the foam is assumed to be no significantly modified by the dissolution procedure because the copper oxides likely to be formed onto the Cu skeleton are reduced during the annealing treatment performed under reductive (H_2) atmosphere. This annealing treatment has also the advantage to improve the mechanical strength of the Cu foam. However, the dissolved Cu foam must be handled with care, indicating that it is more fragile than the as-received foam.

5. Conclusion

The 3D-architecture of copper foams was described in detail by means of X-ray tomography. It was shown that the immersion of the copper foam in an acidic peroxide solution is an efficient way to decrease the foam thickness and to increase its porosity. Such a foam displaying a high open porosity and a very high specific surface area

appears promising for use as a 3D current collector of Si-based anodes for Li-ion batteries (work in progress).

Acknowledgements

Financial funding from the Natural Science and Engineering Research Council (NSERC) of Canada is acknowledged. The authors thank D. Pilon (Metafoam Inc.) for supplying the Cu foams and B. Stansfield (INRS-EMT) for his very helpful comments during the preparation of this article.

References

1. Lefebvre LP, Banhart J, Dunand DC. Adv Eng Mater 2008; 10:775.
2. Li H, Cheng F, Zhu Z, Bai H, Tao Z, Chen J. J Alloys Compd 2011; 509:2919.
3. Li Q, Hu S, Wang H, Wang F, Zhong X, Wang X. Electrochim Acta 2009; 54:5884.
4. Nam DH, Kim RH, Han DW, kwon HS. Electrochim Acta 2012; 66:126.
5. Jiang T, Zhang S, Qiu X, Zhu W, Chen L. Electrochem Commun 2007; 9:930.
6. Shirazy MRS, Fréchette LG. Int J Heat Mass Tran 2013; 58:282.
7. Gauthier M, Lefebvre LP, Thomas Y, Bureau MN. Mater Manuf Process 2004; 19:793.
8. Buffiere JY, Maire E, Adrien J, Masse JP, Boller E. Exp Mech 2010; 50:289.
9. Maire E, Buffiere JY, Salvo L, Blandin JJ, Ludwig W, Létang JM. Adv Eng Mater 2001; 3:539.
10. Maire E, Fazekas A, Salvo l, Dendievel R, Youssef S, Cloetens P, Létang JM. Compos Sci Technol 2003; 63:2431.
11. Elmoutaouakkil A, Salvo L, Maire E, Peix G. Adv Eng Mater 2002; 4:803.
12. Morales-Rodrigez A, Reynaud P, Fantozzi G, Adrien J, Maire E. Scripta Mater 2009; 60:388.
13. Bart-Smith H, Bastawros AF, Mumm DR, Evans AG, Sypeck DJ, Wadley HNG, Acta Mater 1998;46:3583
14. Babout L, Mummery PM, Marrow TJ, Tzelepi A, Withers PJ. Carbon 2005; 43:765.

15. Saadatfar M, Garcia-Moreno F, Hutzler S, Sheppard AP, Knackstedt MA, Weaire D. Colloid Surface A 2009; 344:1077.

16. Loretz M, Maire E, Baillis D. Adv Eng Mater 2008; 10 :352.

17. Shearing PR, Howard LE, Jørgensen PS, Brandon NP, Harris SJ. Electrochem Commun 2010; 12:374.

18. Haibel A, Manke I, Melzer A, Banhart J. J Electrochem Soc 2010; 157:A387.

19. Kehrwald D, Shearing PR, Brandon NP, Sinha PK, Harris SJ. J Electrochem Soc 2011; 158:A1393.

20. Yufit V, Shearing P, Hamilton RW, Lee PD, Wu M, Brandon NP. Electrochem Commun 2011; 13:608.

21. Chen-Wiegart YCK, Shearing P, Yuan Q, Tkachuk A, Wang J. Electrochem Commun 2012; 21:58.

22. Shearing PR, Brandon NP, Gelb J, Bradley R, Withers PJ, Marquis AJ, Cooper S, Harris SJ. J Electrochem Soc 2012; 159:A1023.

23. Yan B, Lim C, Yin L, Zhu L. J Electrochem Soc 2012; 159:A1604.

24 Ebner M, Marone F, Stampanoni M, Wood V. Science 2013; 342:716.

25 Ebner M, Marone F, Stampanoni M, Wood V. Adv Energy Mater 2013; 3:845

26 Liu Z, Cronin JS, Chen-Wiegart YCK, Wilson JR, Yakal-Kremski KJ, Wang J, Faber KT, Barnett SA. J Power Sources 2013; 227:267.

27. Chen-Wiegart YCK., Liu Z, Faber KT, Barnett SA, Wang J. Electrochem Commun 2013; 28:127

28. Caty O, Maire E, Youssef S, Bouchet R. Acta Mater 2008; 56:5524.

29. Madi K, Forest S, Boussuge M, Gailliège S, Lataste E, Buffiere JY, Bernard D, Jeulin D. Comp Mater Sci 2007; 39:224.

30. Youssef S, Maire E, Gaertner R. Acta Mater 2005; 53:719.

31. Cnudde V, Boone MN. Earth-Sci Rev 2013; 123:1.

32. Cakir O. J Mater Process Tech 2006; 175:63.

33. Hu L, La Mantia F, Wu H, Xie X, McDonough J, Pasta M, Cui Y. Adv Energy Mater 2011; 1:1012.

34. Thorat IV, Stephenson DE, Zacharias NA, Zaghib K, Harb JN, Wheeler DR. J Power Sources 2009; 188:592.

35. Reyter D, Rousselot S, Mazouzi D, Gauthier M, Moreau P, Lestriez B, Guyomard D, Roué L. J Power Sources 2013; 239:308.

Table captions

Table 1 Main characteristics of the pores for the as-received and dissolved foams.

Table 2 Main characteristics of the Cu matrix for the as-received and dissolved foams.

Figure captions

Figure 1 SEM micrographs of as-received (A-C) and dissolved (D-F) copper foams on surface (A, D), cross-section (B, E) and at high magnification (C, F).

Figure 2 Thresholding process: (A) Grey-scale X-ray density image of a slice of the untreated foam, (B) Histogram of the grey-level for the full image volume, (C) same slice after binarization into pore and solid phases.

Figure 3 3D reconstructed views of the (A-B) as-received and (C-D) dissolved Cu foams.

Figure 4 Through-thickness porosity mappings in the (xy) and (yz) plans for the (A) as-received and (B) dissolved Cu foams.

Figure 5 Porosity profiles of the as-received and dissolved foams along the (A) x, (B) y and (C) z directions.

Figure 6 X-ray tomography slices perpendicular to z-axis extracted from the volume of the as-received copper foam after the connectivity image processing for the gaseous phase.

Figure 7 Cumulative size distributions of the open- and closed- pores for the as-received and dissolved Cu foams.

Figure 8 Thickness distribution of the copper phase for the as-received and dissolved foams.

Table 1

Sample	Open-porosity (%)	Closed-porosity (%)	Open-pore sphericity	Closed-pore sphericity	Open-pore median size (μm)	Closed-pore median size (μm)	Tortuosity
As-received	71.1	1.0	0.07	0.66	54	6	1.04
Dissolved	81.8	0.3	0.14	0.78	93	5.5	1.03

Table 2

Sample	Specific surface area		Sphericity	Median thickness (μm)	Tortuosity
	m^2/m^3_{foam}	m^2/m^3_{Cu}			
As-received	~74,000	~260,000	0.02	14.5	1.19
Dissolved	~49,000	~280,000	0.03	14.5	1.23

Fig. 1

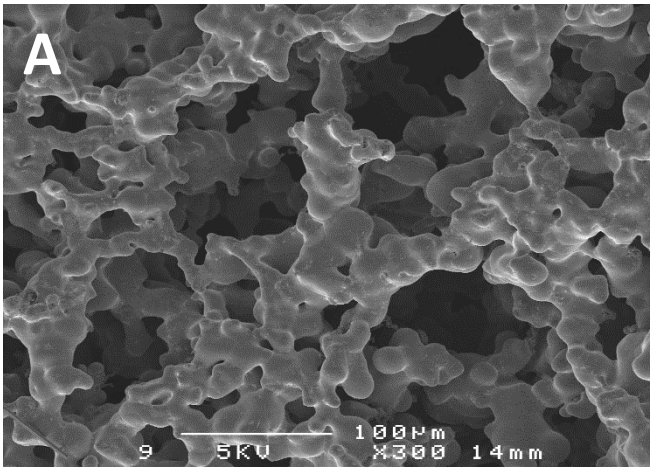
A
100µm
9 5KV X300 14mm

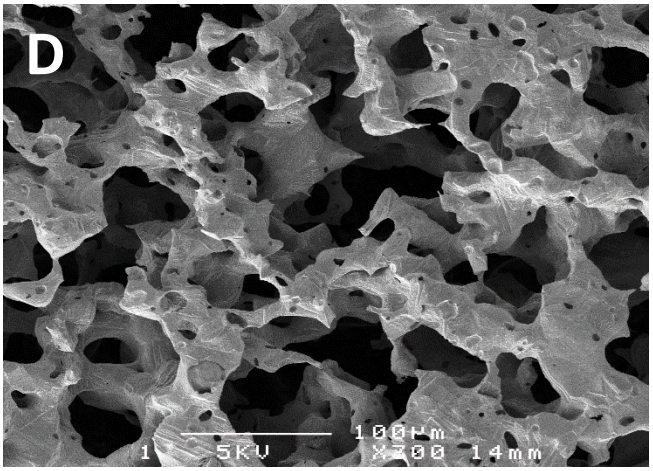
D
100µm
1 5KV X300 14mm

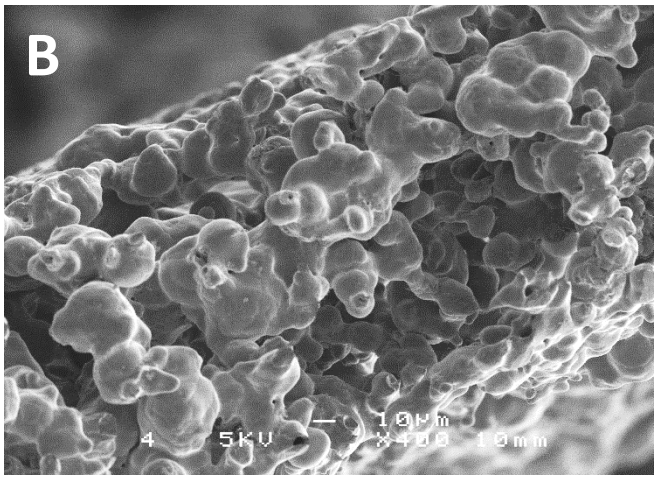
B
10µm
4 5KV X400 10mm

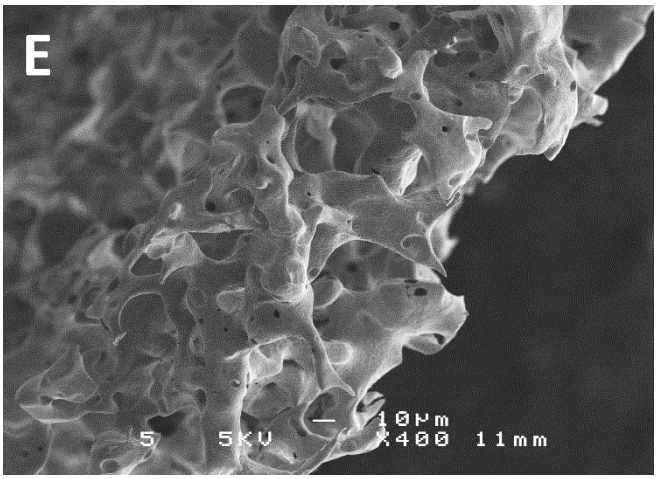
E
10µm
5 5KV X400 11mm

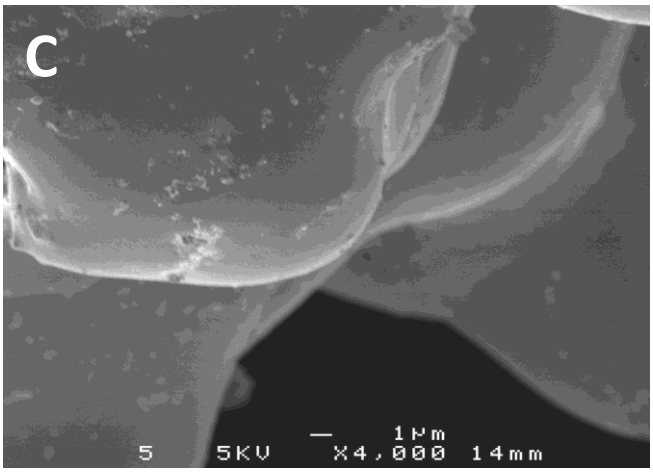
C
1µm
5 5KV X4,000 14mm

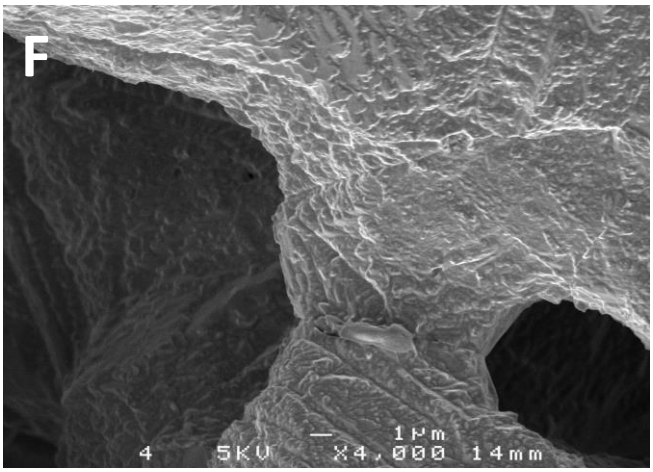
F
1µm
4 5KV X4,000 14mm

Fig. 2

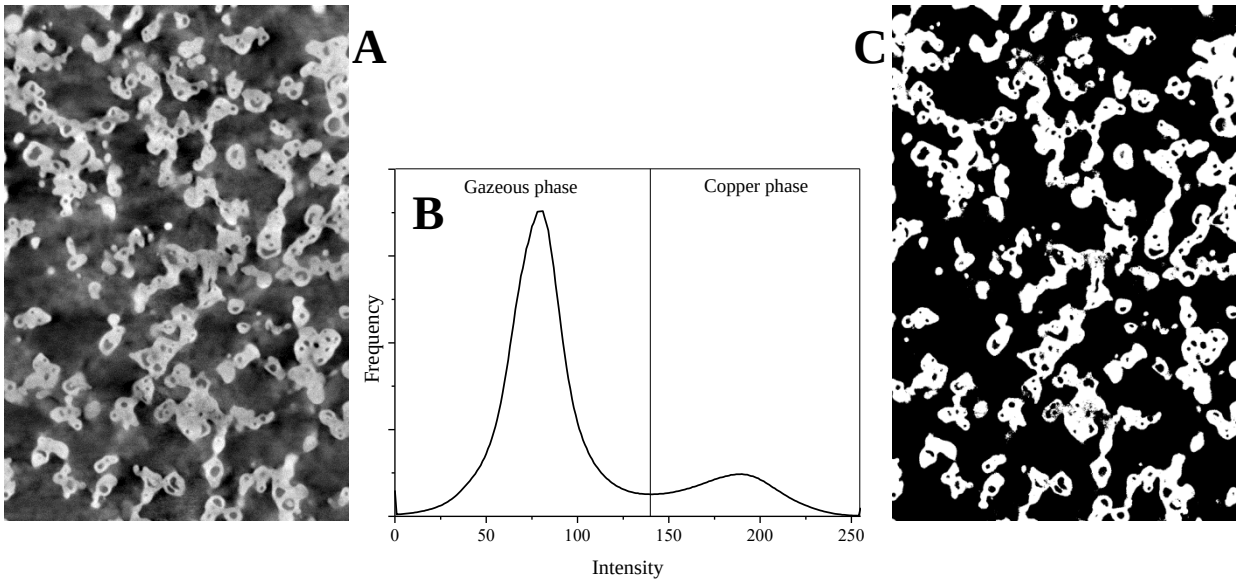
A
B
C
Gazeous phase
Copper phase
Frequency
0
50
100
150
200
250
Intensity

Fig. 3

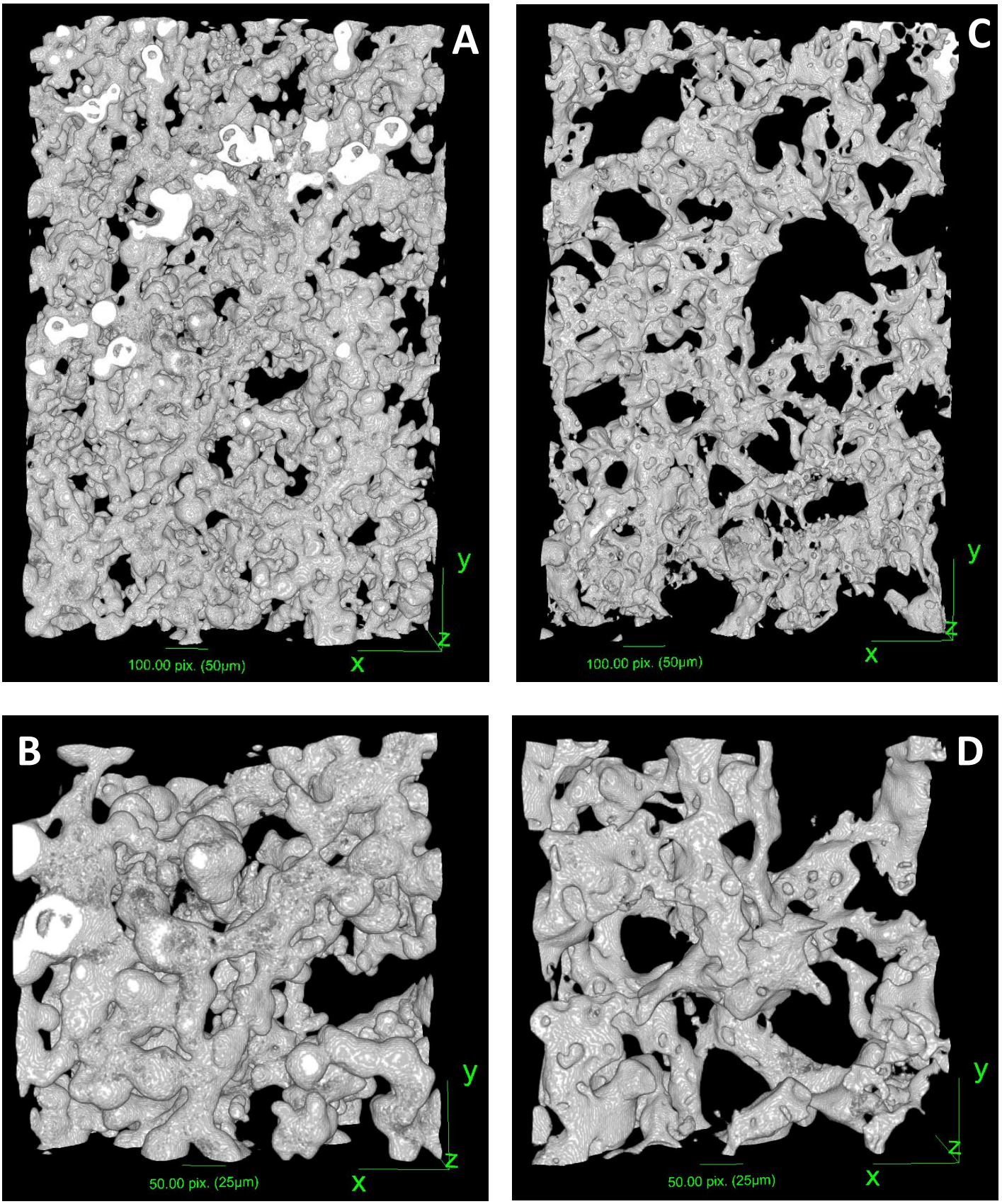
A
y
z
x
100.00 pix. (50µm)
C
y
z
x
100.00 pix. (50µm)
B
y
z
x
50.00 pix. (25µm)
D
y
z
x
50.00 pix. (25µm)

Fig. 4

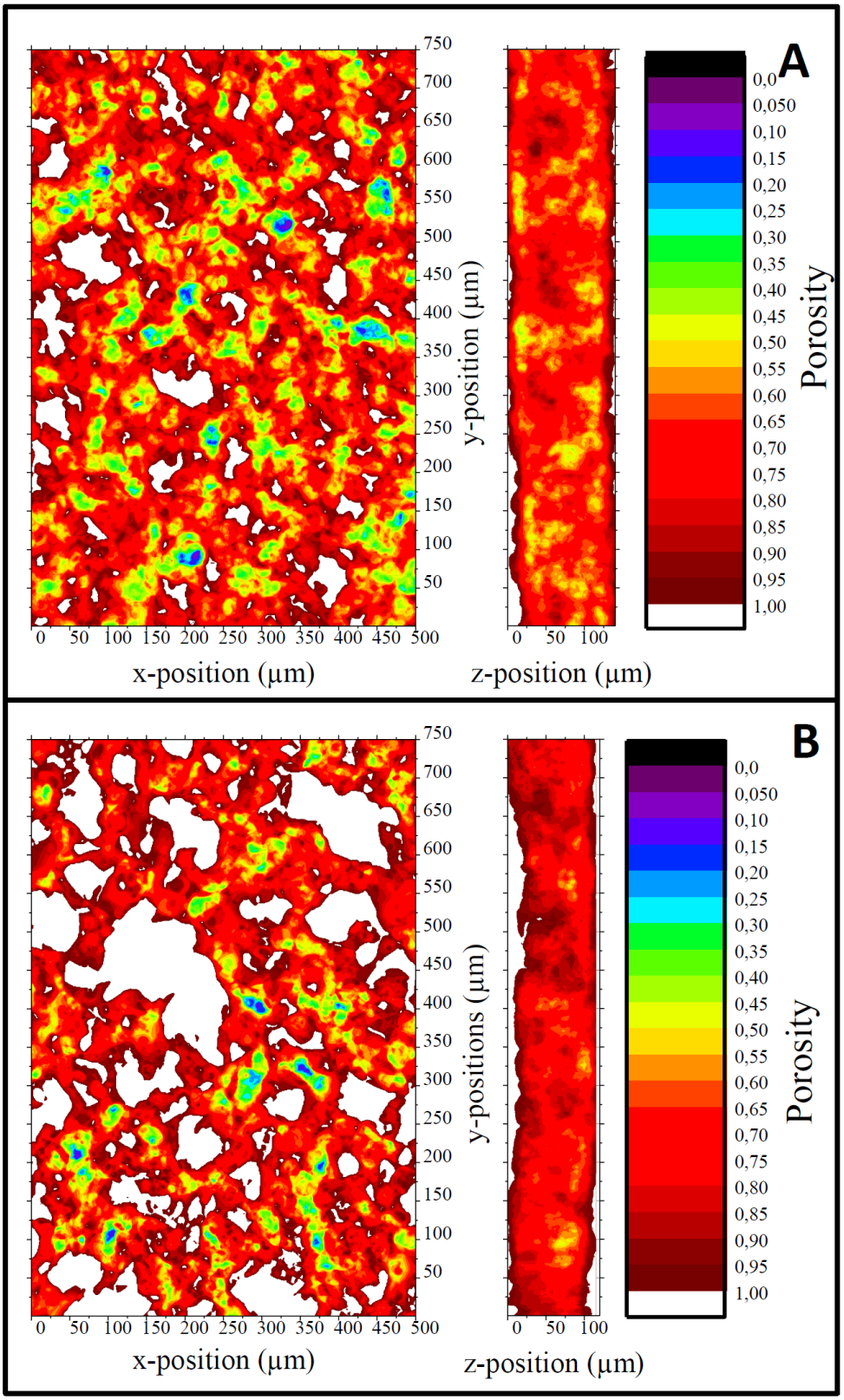
A
B
y-position (µm)
y-positions (µm)
x-position (µm)
z-position (µm)
Porosity
0,0
0,050
0,10
0,15
0,20
0,25
0,30
0,35
0,40
0,45
0,50
0,55
0,60
0,65
0,70
0,75
0,80
0,85
0,90
0,95
1,00
0 50 100 150 200 250 300 350 400 450 500
0 50 100
50 100 150 200 250 300 350 400 450 500 550 600 650 700 750

Fig. 5

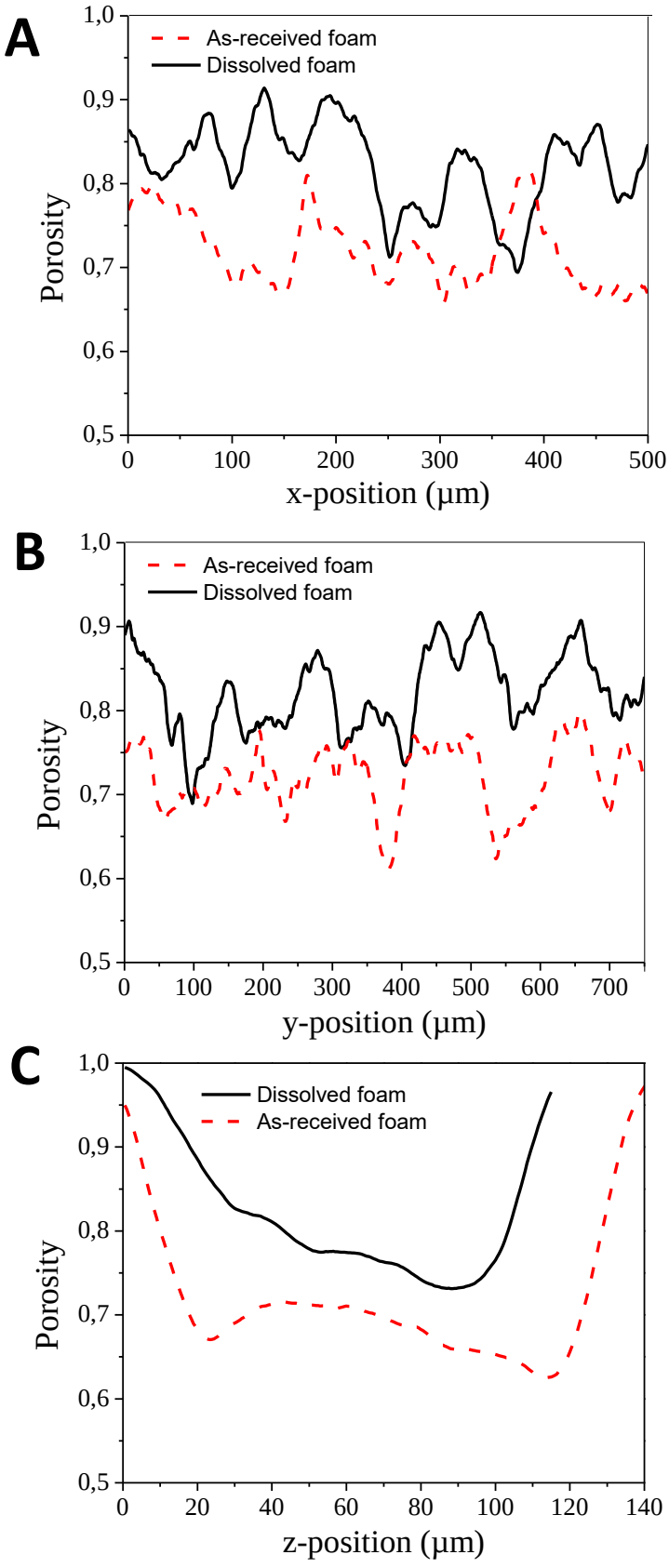
A
As-received foam
Dissolved foam
Porosity
1,0
0,9
0,8
0,7
0,6
0,5
0
100
200
300
400
500
x-position (µm)
B
As-received foam
Dissolved foam
Porosity
1,0
0,9
0,8
0,7
0,6
0,5
0
100
200
300
400
500
600
700
y-position (µm)
C
Dissolved foam
As-received foam
Porosity
1,0
0,9
0,8
0,7
0,6
0,5
0
20
40
60
80
100
120
140
z-position (µm)

Fig. 6

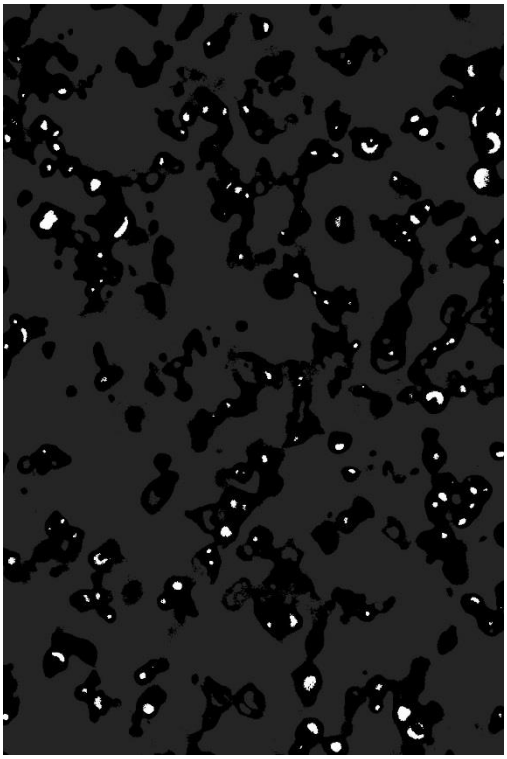

Fig. 7

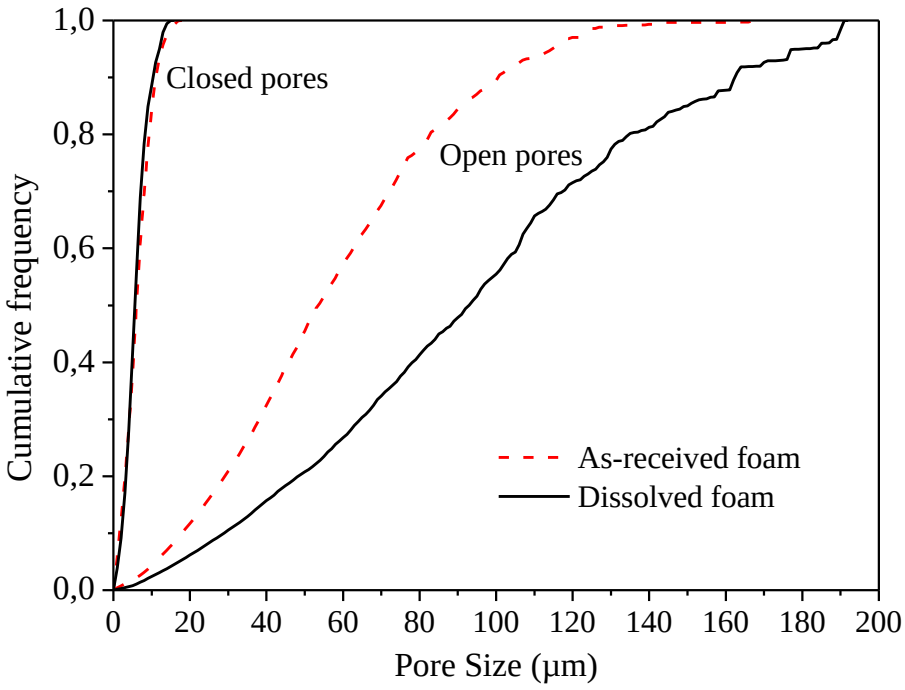
1,0
0,8
0,6
0,4
0,2
0,0
Cumulative frequency
0
20
40
60
80
100
120
140
160
180
200
Pore Size (µm)
Closed pores
Open pores
As-received foam
Dissolved foam

Fig. 8

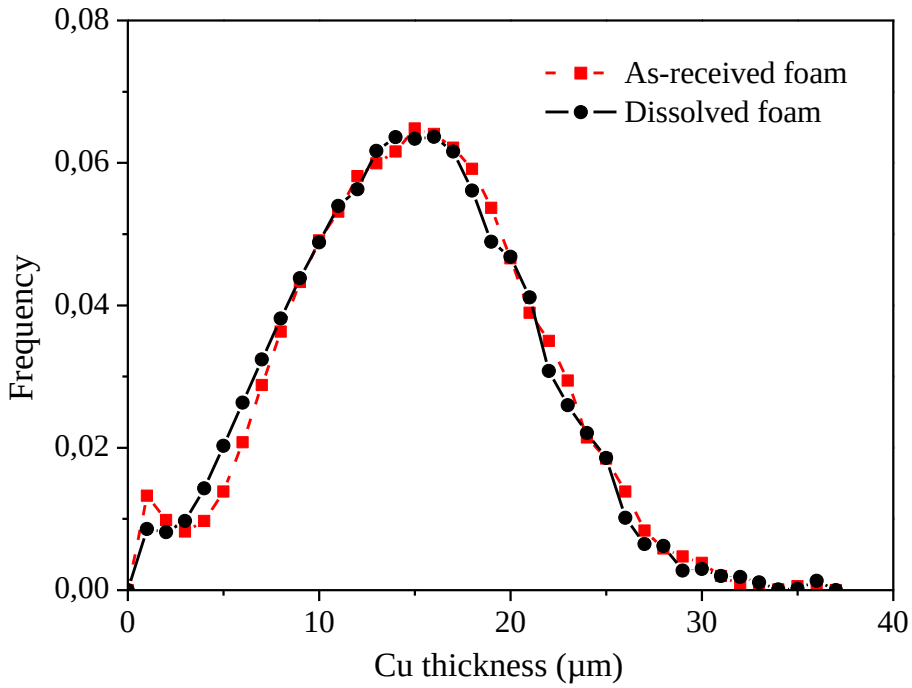
0,08
0,06
0,04
0,02
0,00
Frequency
0
10
20
30
40
Cu thickness (µm)
As-received foam
Dissolved foam